Applied Catalysis B: Environmental 323 (2023) 122143

Contents lists available at ScienceDirect

Applied Catalysis B: Environmental

journal homepage: www.elsevier.com/locate/apcatb

Significant boosting effect of single atom Pt towards the ultrasonic generation of H_2O_2: A two-way catalytic mechanism

Wen Yan [a,c], Jingxiang Sun [a,c], Tao Hu [a,c], Shuanghong Tian [a,c], Jinxi Feng [a,b,*], Ya Xiong [a,c,*]

[a] School of Environmental Science and Engineering, Sun Yat-Sen University, No. 135, Xingang Xi Road, Guangzhou 510275, PR China

[b] Guangdong Provincial Engineering Laboratory of Biomass High Value Utilization, Institute of Biological and Medical Engineering, Guangdong Academy of Sciences, Guangzhou 510316, PR China

[c] Guangdong Provincial Key Laboratory of Environmental Pollution Control and Remediation Technology, Sun Yat-Sen University, No. 135, Xingang Xi Road, Guangzhou 510275, PR China

ARTICLE INFO

Keywords:
H_2O_2
Single atom
Pt
Ultrasound
Catalysis

ABSTRACT

Single atom Pt was anchored on the surface of SiO_2 (Pt_1/SiO_2) with the assistance of ionic liquid. It was found that Pt_1(0.1 %)/SiO_2 could catalyze to sonically generate 3027.1 μmol L^{-1} h^{-1} H_2O_2, being 25.2 folds and 11.6 folds of those from pure ultrasound and sonocatalytic processes of Pt_n(0.1 %)/SiO_2, respectively. It was also the maximum concentration of H_2O_2 generated by sonocatalysis so far. The significant boosting effect of Pt_1 was attributed to the synergetic role of its two-way catalytic processes proved by isotope labeling and DFT calculation. Firstly, Pt_1 catalyzed the sono-splitting of H_2O to generate •OH as the precursor of H_2O_2 formation by increasing the adsorption energy of H_2O; Secondly, it catalyzed the combination of O_2 and •H to selectively generate •OOH as another precursor of H_2O_2 by one end-on type adsorption of O_2 on Pt_1. These findings provided a new way to enhance the ultrasonic generation of H_2O_2.

1. Introduction

Hydrogen peroxide (H_2O_2) is one of the 100 most important chemicals in the world. It is widely utilized in medicine, pulp and textile bleaching, chemical synthesis, semiconductor cleaning, detergent and other applications as an environmentally benign oxidant [1]. Recently, it has still been employed as an emerging high-energy-density liquid fuel for fuel cells to produce electricity [2,3]. Its annual production exceeded 5 million tons in 2015 and is still rising [4]. Currently, over 95 % of H_2O_2 is generated on an industrial scale through the anthraquinone process [5]. However, it cannot be considered to be an ideal process, due to its high energy demand, undesirable by-products and potential explosion hazard from the mixture of H_2 and O_2. These inherent defects of the anthraquinone process have been constantly motivating researchers to develop more efficient, energy-saving and environmentally friendly methods of H_2O_2 production and its versatile synthetic processes have been reported, such as hydrogen-oxygen direct synthesis, two-electron electrochemical oxygen reduction, photocatalytic H_2O oxidation and so on [6].

Since Richards and Loomis discovered the chemical effect of ultrasonic radiation [7], a number of researches on the ultrasonic formation of H_2O_2 have been reported. Although most of them are concerned with the mechanism of ultrasonic splitting of water and ultrasonic degradation of pollutants [8–11], few are still devoted to the ultrasonic synthesis of H_2O_2 [8,12,13]. For example, Ziembowicz investigated the effects of operating conditions on the ultrasonic generation of H_2O_2 in detail [14]. It found that under the optimized conditions, H_2O_2 reached 10 μmol L^{-1}. Sato reported the relationship between ultrasonic frequency and H_2O_2 production rate and proved that frequencies higher than 90 kHz were more effective than low frequencies [15]. Recently, Dalodière found that nitric acid could enhance the ultrasonic production of H_2O_2, and the maximum yield reached 167.6 μmol L^{-1} in nitric solution [16]. However, compared to current H_2O_2 industrial production methods, the efficiency of these ultrasonic generations of H_2O_2 was lower, thus catalysts was introduced into the ultrasonic generation of H_2O_2 [10,17–19]. Presently, the used catalytic materials mainly involve inorganic oxides, such as TiO_2, ZnO, Al_2O_3, quartz and so on [20–22]. Due to the great differences in their experimental conditions, it was difficult to accurately and quantitatively evaluate their catalytic activity, but the aims of all catalytic processes were to increase the production of •OH as an intermediate of H_2O_2 by reaction (1), in which the symbol ')))' standard for the ultrasound.

* Corresponding authors at: School of Environmental Science and Engineering, Sun Yat-Sen University, No. 135, Xingang Xi Road, Guangzhou 510275, PR China.
E-mail addresses: fengjx18@163.com (J. Feng), cesxya@mail.sysu.edu.cn (Y. Xiong).

https://doi.org/10.1016/j.apcatb.2022.122143
Received 31 July 2022; Received in revised form 20 October 2022; Accepted 1 November 2022
Available online 3 November 2022

$$H_2O +))) = \bullet H + \bullet OH \tag{1}$$

$$\bullet OH + \bullet OH = H_2O_2 \tag{2}$$

However, it has been proven that most of these •OH radicals would rapidly recombine with •H to form H_2O inside ultrasonic cavitation bubbles, and only 20 % of them could be coupled to H_2O_2 by reaction (2) [12,16,23]. Therefore, we expected that the capture of •H would be one of the potential pathways to increase the production of H_2O_2, in addition to increasing •OH production. As a rich and low-cost agent, O_2 in the air can not only capture •H radicals but also theoretically produce H_2O_2 via the two-step scavenging reactions (3)–(4) [24]. Unfortunately, the rate of the capturing reaction (1.9×10^{10} mol L^{-1} S^{-1}) is comparable to the self-coupling rate of •H to H_2 (1.4×10^{10} mol L^{-1} S^{-1}) (reaction (5)) [25,26], limiting the generation of H_2O_2 by reactions (3)–(4), thus, the introduction of catalysts towards activating O_2 is a possible alternative strategy to accelerate the rate of reaction (3) and finally increase ultrasonic generation of H_2O_2.

$$O_2 + \bullet H = \bullet OOH \tag{3}$$

$$\bullet OOH + \bullet H = H_2O_2 \tag{4}$$

$$\bullet H + \bullet H = H_2 \tag{5}$$

$$O_2 + H^+ + e^- = \bullet OOH \tag{6}$$

Since Zhang reported the high catalytic activity of atomically dispersed Pt (Pt_1) on FeO_x towards CO oxidation [27], single atom catalysis has attracted much attention because it can provide more uniform, well-defined active sites, compared with common heterogeneous catalysts. In single atom catalysts, Pt_1 has been paid special concerns because it can not only dramatically reduce the usage requirements of expensive and rare Pt [28–37], but also can selectively activate O_2 to produce H_2O_2 by a two-electron electrochemical reduction due to the special one end-on adsorption model of O_2 on Pt_1, in which •OOH as its intermediate [38,39]. While the two end-on adsorption model of O_2 on the surfaces of bulk or nano Pt (Pt_n) catalyst weakens the O=O double bond, facilitating the formation of intermediate •O radical and the generation of H_2O by a four-electron reduction, as shown in Fig. S1 [40,41]. Although the ultrasonic generation of H_2O_2 does not involve the one-electron electrochemical reduction of O_2, the special one end-on adsorption model of O_2 may be also beneficial to the •H-selective reduction of O_2 into •OOH by reaction (3), based on the similarity of reaction (3) and (6). However, so far, there is no report on the catalytic role of Pt_1 towards ultrasonic generation of H_2O_2. Motivated by the above possible beneficial effect, we initiated the project on the ultrasonic production of H_2O_2 catalyzed by Pt_1, in an attempt to enhance its yield.

Herein, this paper will focus on investigating the ultrasonic generation of H_2O_2 in the presence of catalyst Pt_1 anchored on SiO_2 (Pt_1/SiO_2). These investigations mainly include the preparation and characterization of Pt_1 on SiO_2, the enhancement effect of Pt_1 on the ultrasonic generation of H_2O_2, its dependence on operation conditions, and so on. Special attention will be paid to finding and identifying the new catalytic mechanism of Pt_1 towards the ultrasonic generation of H_2O_2, including the related ultrasonic cracking of H_2O and activation of O_2, in addition to its usual high dispersion, in order to understand the catalytic performance of Pt_1.

2. Experimental

2.1. Material and reagents

Platinum(II) acetylacetonate (Pt(acac)$_2$), 1-Butyl-3-methylimidazolium bis (trifluoromethylsulfonyl) imide ([Bmim][Tf$_2$N]), sodium hydroxide (NaOH), tetrachloromethane (CCl_4), chloroplatinic acid hexahydrate ($H_2PtCl_6 \cdot 6H_2O$), 5,5dimethyl-1-pyrroline N-oxide (DMPO), 2,2,6,6-tetramethylpiperidine (TEMP), luminol ($C_8H_7N_3O_2$), and methanol were all obtained from Shanghai Macklin Biochemical Co., Ltd. Silicon dioxide (SiO_2) and potassium iodide (KI) were bought from Aladdin Chem. Co., Ltd. Acetone, ethanol, H_2O_2 (30 %), potassium biphthalate ($C_8H_5O_4K$), and ammonium molybdate ($(NH_4)_2MoO_4$) were purchased from Guangzhou Chemical Reagent Factory (China). Argon and oxygen were provided by Foshan MS Messer Gas Co., Ltd (China). All reagents were of analytical grade and used without further purification. Deionized water was used throughout all experiments (pH ≈ 6.5).

2.2. Instrument and measurement

X-ray diffraction (XRD) patterns of Pt/SiO_2 powders were obtained with a D-MAX 220 VPC diffractometer (Rigaku Corporation, Japan) with Cu Kα radiation at 40 kV and 30 mA. Transmission electron microscopy (TEM) and high-resolution transmission electron microscopy (HRTEM) images were provided by the JEOL JEM-2010HR instrument. High-angle annular dark-field scanning transmission electron microscopy (HAADF-STEM) images and elemental mapping of samples were performed using FEI Titan 60–300 electron microscope equipped with a spherical aberration corrector and energy dispersive X-ray spectroscopy (EDX). The Pt amounts were determined by inductively coupled plasma mass spectrometry (ICP-MS, Perkin Elmer NexION 350D). X-ray photoelectron spectroscopy (XPS) measurements were carried out at ESCALAB 250, Thermo-VG Scientific (UK) system with advantage software for data acquisition and analysis. The Pt L_3-edge X-ray absorption spectroscopy (XAS) spectra that include extended X-ray absorption fine structure (EXAFS) and X-ray fine near-edge structure (XANES) was measured at the XAS station (BL14W1) of the Shanghai Synchrotron Radiation Facility (SSRF). The XAS data were analyzed and fitted with the IFEFFIT software packages that include Athena and Artemis. Fourier transform infrared (FTIR) spectra in the 4000–400 cm^{-1} frequency range were obtained using the KBr pellet technique on a Vertex 70 v Hyperion 3000. The BET data of the samples were obtained after the physical adsorption of N_2 at 77.3 K using an auto-adsorption machine (ASAP 2460). Electron paramagnetic resonance (EPR) spectra were recorded on Bruker EMX plus under irradiation of ultrasonication. For the detection of •H and •OH radicals overlap spectrum, DMPO as the spin trapping reagent, and the catalyst was suspended in H_2O/DMPO (20 mmol L^{-1}) mixture solution under Ar atmosphere. The individual spectrums of •OH and •H were detected in H_2O/CCl_4 (20 mmol L^{-1}) and methanol/H_2O (V: V = 60 %) solutions with the addition of DMPO (20 mmol L^{-1}) under the Ar atmosphere, separately. •OOH and $^1O_2$ radicals were determined in the Ar(80 %)-O_2(20 %) atmosphere with methanol/H_2O (V: V = 60 %) and TEMP/H_2O (20 mmol L^{-1}) solutions, respectively [20,42–44] ·H_2O_2 concentration was determined by the KI dosimetry method (limit of detection ≈10^{-6} mol L^{-1}) [45]. The photographs of sonochemiluminescence (SCL) were captured with a digital camera. The experiment was carried out under the irradiation of ultrasonic and 50 mg catalyst was suspended in 50 mL luminol solution (100 mmol L^{-1} NaOH and 2 mmol L^{-1} luminol) [46]. The oxygen isotope of H_2O_2 was determined with the method reported by Joel, that is, H_2O_2 was oxidized by $KMnO_4$ to O_2 and then the isotopes of these O_2 were analyzed with a mass spectrometer (Finnigan MAT-271) [47]. The density functional theory (DFT) calculations were carried out using the Vienna Ab-initio Simulation Package (VASP) with the frozen-core all-electron projector-augment-wave (PAW) method [48–50].

2.3. Preparation of Pt/SiO_2

Pt_1/SiO_2 was prepared with reference to an impregnation-reduction method reported by Ding [51]. Stoichiometric amounts of Pt(acac)$_2$ were dispersed by 5 mL of acetone and then stirred to mix thoroughly. SiO_2 was pretreated in an oven at 100 ℃ for 1 h to remove adsorbed water and then added to the above solution. Next, the slurry was stirred

at a rate of 600 rpm at room temperature until the acetone solution was completely evaporated. The obtained powders were transferred into an oven to dry at 100 ℃ in the air for 1 h. To stable single atom Pt on SiO_2, the above powders and ionic liquids [Bmim][Tf_2N] (the molar ratio of Pt to [Bmim][Tf_2N] was 1:6) were added to 4 mL methanol. The mixture was irradiated using a high-pressure mercury lamp (main wavelength 365 nm, 500 W) for 30 min under sonication and then stirred at a rate of 600 rpm under room temperature until methanol was completely evaporated. Finally, the resulting powder was calcined in a muffle furnace under an air atmosphere at 200 ℃ for 1 h. Nano Pt loaded on SiO_2 (Pt_n/SiO_2) was prepared by the usual photo-reduction deposition of H_2PtCl_6 [44]. In a typical synthesis, SiO_2 was dispersed in 50 mL ethanol aqueous solution (50 %), then stirred well. An H_2PtCl_6 solution according to the stoichiometric ratio was introduced into the above aqueous under stirring for 30 min. The dispersion was subjected to the Xenon lamp (PLS-SXE 300 +, 300 W) treatment for 1 h under sonication. Finally, the sample was centrifuged, washed with deionized water several times, and dried at 100 ℃ for 24 h.

2.4. Ultrasonic generation of H_2O_2

Ultrasonic generation of H_2O_2 was performed in a 250 mL beaker in a commercial 40 kHz, 20 W ~ 120 W ultrasonic cleaner (Skymen, JM-03D-40). Typically, 50 mL of deionized water (pH ≈ 6.5) along with 50 mg of catalyst was used in the experiments. Cooling circulating water was used to maintain the bath temperature at 20 ± 3 ℃. Samples were taken out at 10 min intervals and filtered with 0.22 μm PTFE syringe filters. Generally, the ultrasonic generation of H_2O_2 was performed in an air atmosphere, unless otherwise specified.

3. Results and discussion

3.1. Characterization of Pt_1/SiO_2

The heterogeneous catalyst Pt/SiO_2 was prepared by the impregnation-reduction of $Pt(acac)_2$ with the assistance of an ionic liquid. Considering the loading amount of Pt was a crucial factor to obtain Pt_1/SiO_2 with atomic dispersion and desirable catalytic performance [52], Fig. 1a presented the XRD of the as-prepared Pt/SiO_2 with various loading amounts. When the amount of Pt was greater than or equal to 0.45 %, the two small characteristic peaks were observed at 2θ = 39.7° and 46.2°, being consistent with the XRD diffraction peaks of (111) and (200) planes of Pt^0, respectively. Their averaged sizes of Pt species corresponding to 0.45 %, 0.94 %, 1.33 %, 1.56 %, and 3.86 % of Pt loading amount were calculated by Scherrer's equation as 2.5 nm, 3 nm, 4.5 nm, 5 nm and 5.5 nm, respectively, and the color of samples changed gradually from white to gray and finally to brown (Fig. 1b). When the loading amounts of Pt was lower than 0.45 %, no apparent peaks of Pt were observed in the XRD spectra. However, the EDS mapping of Pt(0.1 %)/SiO_2 revealed the existence of Pt on the surface of SiO_2, as indicated in Fig. 1c. These results denoted that these Pt species were possibly too less or Pt particle was too tiny for the determination of XRD. The inference was further confirmed by HAADF-STEM, XPS, and so on.

As shown in Fig. 2a and b, although no Pt species could be still observed on TEM and STEM images of Pt(0.1 %)/SiO_2 sample, the HAADF-STEM image (Fig. 2c) presented many bright spots with a size of less than 0.18 nm Pt (marked with yellow circles), being similar to that of Pt_1 reported by Zeng [53,54]. The similarity suggested these Pt species were possibly anchored on the surface of SiO_2 in the form of isolated single atom Pt_1 [55–57]. Moreover, no cluster bright spot was found in randomly selected different regions in HAADF-STEM, demonstrating that all, at least, most Pt species were possible atomically dispersed on SiO_2.

To further confirm the occurrence of the atomically dispersed Pt_1 and clarify its coordination environment and chemical state, XAS analysis was performed. From the EXAFS spectra (Fig. 3a and c), it could be found that there was one prominent peak of Pt-O contribution at ~1.7 Å in Pt(0.1 %)/SiO_2. The distance of Pt-O coordination (2.04 ± 0.03 Å) (Table S1) was much closed to the reported distance (2.02 Å) of Pt-O coordination in Pt single atom/FeO_x [27], and moreover, no signal of Pt-Pt contribution, like that of Pt foil (Fig. 3a and e) was observed between 2.5 and 3.0 Å. These facts indicated again that Pt species in Pt(0.1 %)/SiO_2 were basically atomically dispersed and anchored on the surface of SiO_2. Thus, Pt(0.1 %)/SiO_2 could be regarded as Pt_1(0.1 %)/SiO_2. The result was consistent with that of the HAADF-STEM observation.

For Pt(0.45 %)/SiO_2 sample, although the EXAFS peaks of Pt-O and Pt-Pt contribution were both observed at ~1.7 Å and 2.76 Å, individually, the peak intensity of Pt-Pt contribution was much stronger than Pt-O contribution, as shown in Fig. 3a and d. These EXAFS features suggested that these Pt(≥ 0.45 %)/SiO_2 samples contained more clusters or nano Pt with greater sizes, in addition to a few Pt-O. Moreover, the coordination number of these Pt-O contributions was only 1.7, much less than that (5.2) of Pt-O contributions in Pt(0.1 %)/SiO_2 sample. This great discrepancy suggested that the coordination environment of Pt-O in Pt(≥ 0.45 %)/SiO_2 was much different from that of single atom Pt-O in Pt(0.1 %)/SiO_2, although they were both observed at ~1.7 Å. In addition, it was still observed from XANES spectra (Fig. 3b) that the white line peak intensity of the Pt(0.1 %)/SiO_2 sample was stronger than that of Pt foil and also slightly stronger than that of Pt(0.45 %)/SiO_2. This fact indicated that these single atoms Pt in Pt(0.1 %)/SiO_2 were electron deficiency [27,51,58,59], compared to those in Pt(0.45

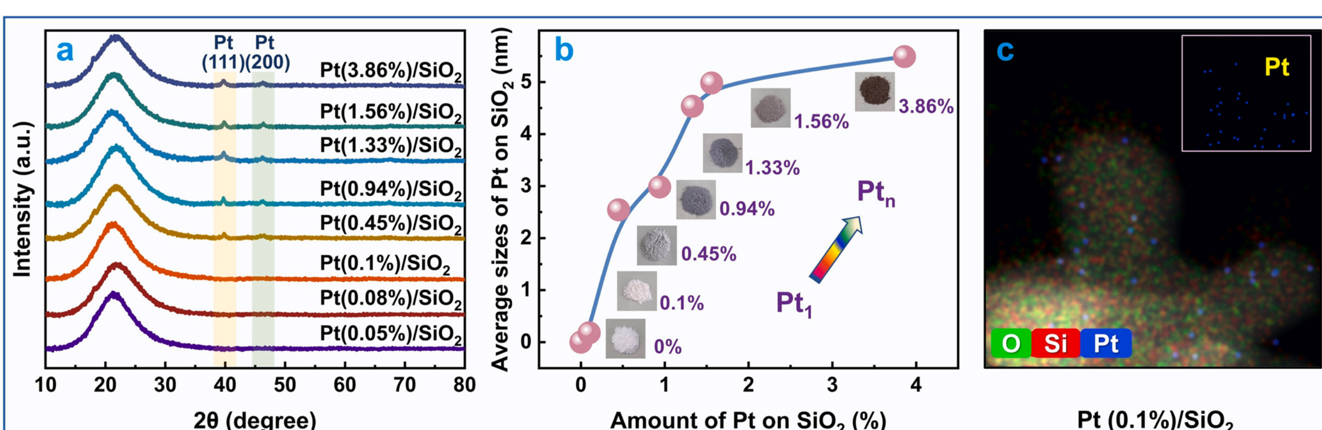

Fig. 1. Characteristics of Pt species in Pt/SiO_2 (a: XRD patterns with various loadings, b: particle sizes of Pt species on SiO_2 with various loading amounts, and c: EDS mapping of Pt(0.1 %)/SiO_2; the percentage in Pt(%)/SiO_2: the loading amount of Pt).

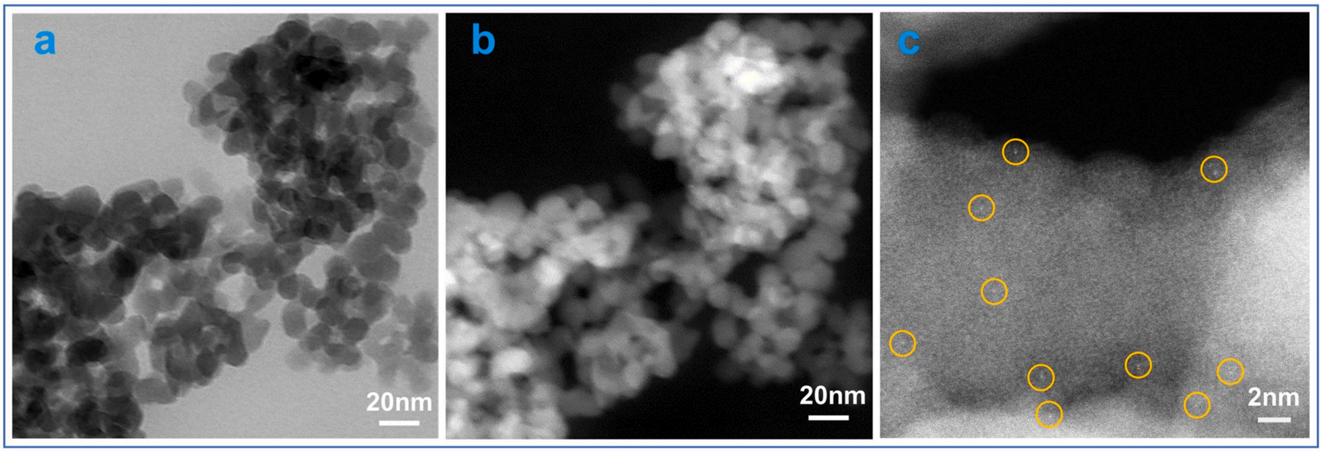

Fig. 2. Morphology and structure characterizations of Pt_1(0.1 %)/SiO_2 (a: TEM image, b: STEM image, c: HAADF-STEM image; the percentage in parentheses represented the loading amount of Pt).

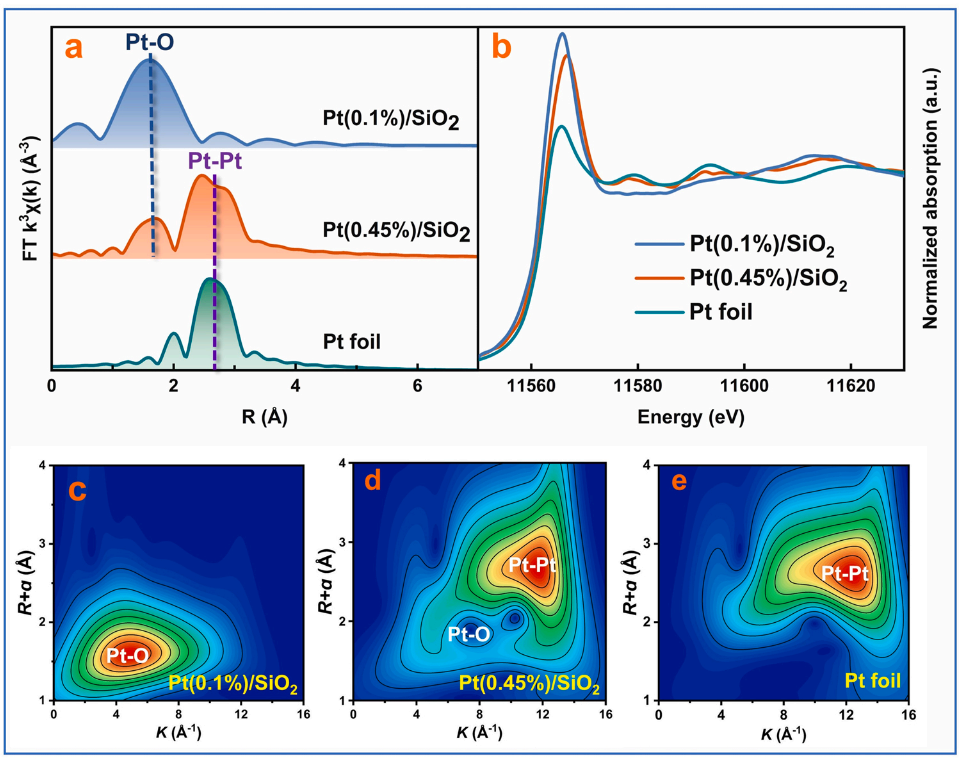

Fig. 3. X-ray absorption spectroscopy of various Pt materials (a: k^3-weighted fourier transform spectra from EXAFS, b: normalized XANES spectra at Pt L_3-edge, c-e: wavelet-transform (WT) of Pt k^3-weighted EXAFS signals).

%)/SiO_2 and Pt foil. This denoted that the electric effect of single atom Pt in Pt(0.1 %)/SiO_2 was different from that of Pt in Pt($\geq$ 0.45 %)/SiO_2, although they were both these single atoms Pt existed in the form of $Pt^{\delta+}$.

To further know information on the chemical states of Pt in Pt/SiO_2, samples with various loading amounts of Pt were analyzed with XPS spectra. Unfortunately, for Pt/SiO_2 with a loading amount of < 0.45 %, no XPS characteristic peaks of Pt were observed possibly since the content of Pt was too low. XPS spectra of other samples were presented in Fig. S2. Two kinds of chemical states Pt (Pt^0 and $Pt^{\delta+}$) were observed from these figures. Referring to the reported method of estimating content by XPS by Bera [60], it was found that the content of Pt^0 was linearly increased with Pt loading amount in the range of low loading amount, and the intercept of the line was much closed to 0.1 % (Fig. S2f). This result further confirmed that for Pt/SiO_2 sample with < 0.1 % loading amount, all Pt species existed in $Pt^{\delta+}$ and no Pt^0, being consistent with the result obtained from analysis of XAS. Moreover, it could be still seen from these XPS spectra that the binding energies of $4f_{7/2}$ and $4f_{5/2}$ of these $Pt^{\delta+}$ species were located in the range of 73.08–73.55 eV and 76.10–76.74 eV, respectively. The binding energies of these 4 f were slightly higher than those of single atom Pt^{2+} reported by He [61] but much closed to those of single atom Pt^{2+} reported by Wang [62,63]. Combined with the above results from the HAADF-STEM image, XAS, and XPS analysis, it could be inferred that the atomic-scale decoration of Pt on SiO_2 could be achieved below 0.1 % loading amount by the present method and they basically existed in the form of Pt^{2+}. Referring to Xu's research [64], the occurrence of these Pt^{2+} with the positive charge and Pt-O binding in these Pt_1/SiO_2 samples indicated

there were strong interactions between these Pt_1 species and adsorbed O_2 from the air, in addition to the SiO_2 surface. This strong interaction was possibly beneficial to the generation of H_2O_2 by O_2 activation.

Based on the above characterizations, in the following research, much attention would be paid to Pt(0.1 %)/SiO_2 sample because it existed basically in Pt_1/SiO_2 form with a higher loading amount. But, in order to compare the catalytic activities between the Pt_1/SiO_2 and Pt_n/SiO_2 with the identical loading amount, the Pt_n(0.1 %)/SiO_2 sample with a similar surface area (153.6 m^2 g^{-1}) to Pt_1(0.1 %)/SiO_2 (129.2 m^2 g^{-1}) was also prepared by the usual photo-reduction of H_2PtCl_6 [44]. As shown in Fig. S3a and b, many nano-Pt particles (Pt_n) with the size of about 5 nm on the surface of SiO_2 were obviously observed on the STEM image (marked by yellow circles), although Pt species did not also determine by XRD (Fig. S3c). In addition, Fig. S4 presented the FTIR spectra of SiO_2, Pt_n(0.1 %)/SiO_2 and Pt_1(0.1 %)/SiO_2. It could be seen from these figures that for the first two samples, no other FTIR adsorption peaks were observed, except for the peaks of SiO_2, while Pt_1(0.1 %)/SiO_2 presented a set of weak FTIR adsorption peaks between 1500 cm^{-1} - 1600 cm^{-1} and 2800 cm^{-1} - 3200 cm^{-1}. According to Rao's research [65], the absorption bands at about 1575 cm^{-1} corresponded to the ring in-plane symmetric/anti-symmetric stretch, CH_2(N) and CH_3(N) CN stretch of pure [Bmim][Tf_2N], and the weak FTIR adsorption peaks between 2800 cm^{-1} and 3200 cm^{-1} could be attributed to that of aliphatic C-H groups in the methyl and butyl moieties of [Bmim][Tf_2N]. These facts suggested that the ionic liquid remained on the surface of SiO_2 acting as a stabilizer of Pt_1 as reported by Ding [51].

3.2. Strongly boosting effect of Pt_1 on the ultrasonic generation of H_2O_2

It has been known from the above characterization that the existing form of Pt species on SiO_2 was intensively related to its loading amount of Pt. Accordingly, the dependence of H_2O_2 generation on the loaded amount of Pt was first investigated as shown in Fig. 4a. The concentration of H_2O_2 increased rapidly with Pt loading amount, reached a maximum value at 0.1 % and then decreased, showing a volcanic-like curve. The maximum H_2O_2 concentration was 829.5 μmol L^{-1}, being 48.5 folds of H_2O_2 concentration for only carrier SiO_2 (17.1 μmol L^{-1}). Due to the H_2O_2 concentration for the only carrier SiO_2 being only slightly higher than that (8.5 μmol L^{-1}) for pure ultrasound (without catalyst and carrier), it could be inferred that the above enhancement of H_2O_2 generation for Pt/SiO_2 originated from Pt, not from SiO_2, and SiO_2 only acted as the carrier of Pt.

For the sake of well understanding the volcanic-like change of H_2O_2 concentration with Pt amount, the effect of the size of these loaded Pt species on H_2O_2 generation was also shown in Fig. 4b. The concentration of H_2O_2 rapidly decreased with the increase of Pt particle size, showing an obvious size effect. Moreover, the closer the size was to that of Pt_1, the more obvious the size effect was. Namely, Pt_1 possessed the best catalytic activity toward the ultrasonic generation of H_2O_2. According to the above characterization results of the loaded Pt, the optimal content of Pt_1 formation was 0.1 %, and over this loading amount, Pt started agglomeration and the content of Pt_1 was reduced. Therefore, the volcanic-like nonlinear change of Fig. 4a could also be considered to be dependent on not only Pt_1 content and Pt species size in these Pt/SiO_2 catalysts. Referring to the present research results about single atom catalysts [66,67], the size effect of Pt catalysts was possibly dependent not only on dependent on not only the difference of their active site number but also their coordination environment and electric effect as indicated in the above XAS and XPS spectra.

Fig. 4c presented the kinetic curves of H_2O_2 generation in the presence of Pt_1 and Pt_n with identical loading amounts to further comprehend the enhancement effect of Pt_1. The concentration of H_2O_2 both increased linearly with time and displayed zero-order kinetic features for Pt_1(0.1 %)/SiO_2 and Pt_n(0.1 %)/SiO_2, similar to that of H_2O_2 generation in single ultrasonic processes reported by Her [68], but their rate constants were quite different. The rate constant for Pt_1(0.1 %)/SiO_2 was 13.82 μmol L^{-1} min^{-1}, it was 16.4 folds of Pt_n(0.1 %)/SiO_2 (0.84 μmol L^{-1} min^{-1}). These obvious kinetic differences further confirmed that Pt_1 possessed a strongly boosting catalytic effect on the ultrasonic generation of H_2O_2 compared with the same amount of Pt_n.

3.3. Dependence of operation conditions on H_2O_2 generation

To further know the catalytic performance of Pt_1 towards the ultrasonic generation of H_2O_2, the effects of main operation conditions on H_2O_2 generation were also investigated, which included sonic power, water temperature in bath, dissolved gases, reuse times, etc.

Fig. 5a presented the change of H_2O_2 generation with various ultrasonic powers in the presence of Pt_1(0.1 %)/SiO_2. The concentration of their H_2O_2 first increased and reached a maximum at about 40 W and then slowly decreased with ultrasonic power, showing a nonlinear dependence of H_2O_2 generation on the ultrasonic power. The raising phenomenon could be simply attributed to the fact that the number of cavitation bubbles and the temperature within individual cavitation bubbles increased with the increase of ultrasonic power, for a given ultrasound frequency [14,68–70]. Although the decrease seemed somewhat unexpected, it could be still roughly understood from the mechanism of sonoluminescence quenching reported by Asakura and Yasuda [71]. They thought that the traveling wave field would increase and the standing wave field would decrease with increasing ultrasonic power, leading to the reduction of the chemical reaction field, and furthermore, the expansion and the contraction of bubbles produce a phase difference because of the higher sound pressure. As a result, bubbles trapped in the antinodes of the sound pressure of the standing wave by the primary Bjerknes force were repelled, resulting in the number of bubbles decreasing [71]. With the increase of ultrasonic

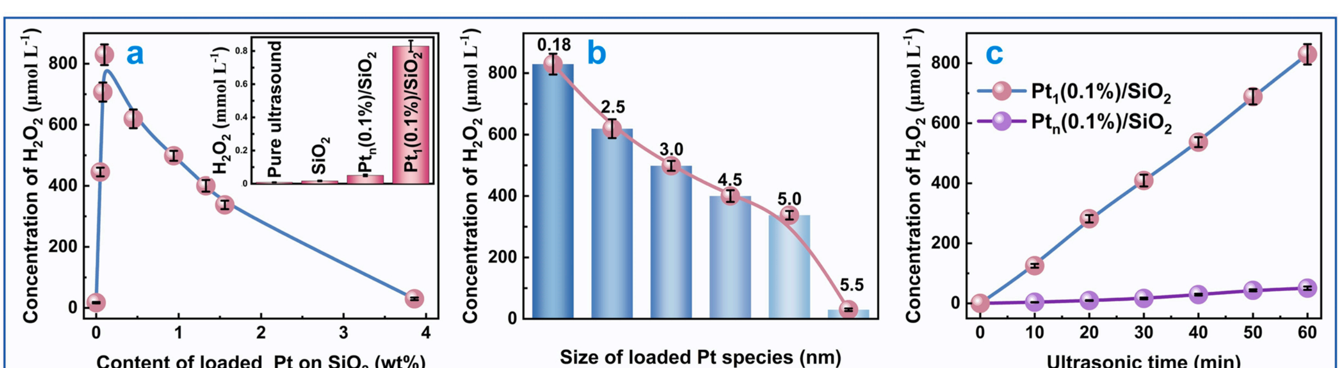

Fig. 4. Sonocatalytic generation of H_2O_2 by Pt/SiO_2 (a: effect of Pt loading amount, b: size effect of Pt species, c: kinetics of H_2O_2 generation; the dosage of Pt/SiO_2: 50 mg; sonication power: 40 W; sonication time: 60 min; temperature: 20 ℃, unless otherwise specified).

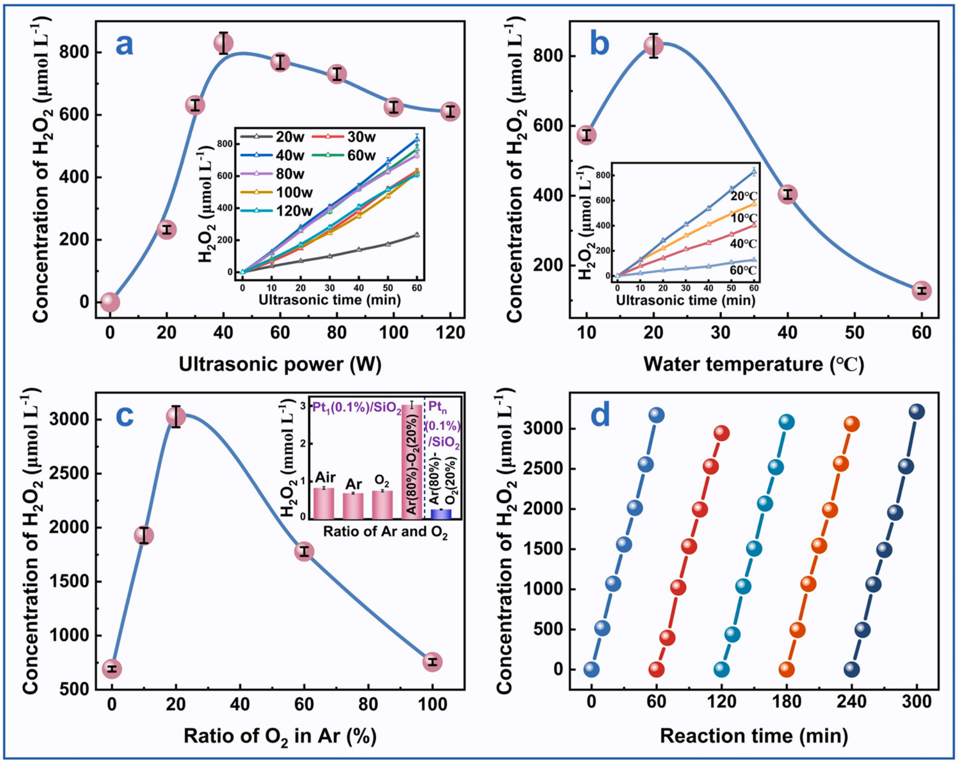

Fig. 5. Effect of ultrasonic conditions on the H_2O_2 generation of Pt_1(0.1 %)/SiO_2 (a: ultrasonic power, b: water temperature in bath, c: different atmosphere, d: reuse times; the dosage of Pt_1(0.1 %)/SiO_2: 50 mg; sonication power: 40 W; sonication time: 60 min; temperature: 20 ℃, unless otherwise specified).

power, the decrease of the chemical reaction field and bubble number might lead to the reduction of H_2O_2 [72]. Fig. S5 showed that the optimal pH range of H_2O_2 sono-catalytic generation was about 5–7, and the increase and decrease of the initial solution pH of the water were unfavorable for the generation of H_2O_2. Therefore, in the present investigation, the pH value of usual water was applied, unless otherwise specified.

The relationship between H_2O_2 generation and water temperature in the ultrasonic bath was shown in Fig. 5b. It could be seen that the concentration of H_2O_2 increased firstly and then decreased with the rising of bulk water temperature, and the optimal water temperature in the ultrasonic bath was about 20 ℃. Previously, the effect of bulk water temperature on ultrasonic reactions had been investigated by some research groups. They presented different experimental results, such as the positive and negative effects and no apparent effect [9,13,73,74]. Referring to Laxmi's view [75], the positive effect at low temperatures (< 40 °C) was due to the higher mass transfer of different species at higher water temperatures and this leads to an enhancement in the rate of H_2O_2 formation reaction outside cavitation bubbles. The negative effect at high temperatures (> 40 °C) was a special phenomenon of ultrasonic reactions. It could be stemmed from two facts: Firstly, with the water temperature increasing, the content of water vapor increased, leading to the increase of the vapor entering the ultrasonic cavitation bubbles during their growth. Due to the cushioning effect of these vapors, the collapsing shock of the cavitation bobbles would be reduced, in other words, the bubble temperature of the ultrasonic 'hot spot' would be reduced [74], resulting in slowing down of H_2O_2 formation. Secondly, the solubility of O_2 was appreciably decreased with the increase in water temperature in the bath. For example, at standard atmospheric pressure, the solubility of O_2 was 11.5 mg L^{-1} at 5 ℃ while it would reduce to 5.47 mg L^{-1} at 50 ℃. Considering that, at least, a pathway of ultrasonic generation of H_2O_2 was directly related to the dissolved O_2 in water, such as O_2 capture of •H radicals (reaction (3)–(4)) [76]. Thus, it was reasonable to believe that the decrease in O_2 solubility was also one of the main factors responsible for the reduction of H_2O_2 production.

To understand more about the role of O_2, Fig. 5c presented the ultrasonic generation of H_2O_2 in the presence of various gases. Unexpectedly, although the generation of H_2O_2 in the O_2 atmosphere was more than in inert Ar gas, it was still less than that in the air, as shown in the insertion diagram in Fig. 5c. This fact further suggested that O_2 was very important for the ultrasonic generation of H_2O_2, but it is not always the case that the more oxygen, the more H_2O_2. The generation of H_2O_2 was significantly enhanced when O_2 was mixed with Ar. As shown in Fig. 5c, with the addition of O_2 in Ar, the concentration of H_2O_2 firstly increased and then decreased, showing a typical volcano appearance, but all concentrations of H_2O_2 in the mixed gases were higher than those in O_2, Ar, and air atmospheres. For the atmosphere with Ar(80 %)-O_2(20 %), the concentration of H_2O_2 reached as high as 3027.1 μmol L^{-1} for 1 h, and while it was just 755.6 μmol L^{-1} and 691.3 μmol L^{-1} in the pure O_2 and Ar, respectively. The former was 4.0 and 4.4 times of the latter two individually. As we know, this was presently reported max concentration of H_2O_2 generated by ultrasonic catalysis so far. As a famous inert gas, Ar generally did not directly participate in the chemical reaction, thus the unexpected enhancement might be understood from its physical effect on ultrasonic cavitation. It was known that monatomic Ar possessed a higher adiabatic index γ (1.67) than diatomic O_2 (1.39). Based on Kanthale's research [70], the maximum temperature of cavitation bubbles was direct to $(R_{max}/R_{min})^{3(\gamma-1)}$, where R_{max} is the maximum radius of the bubble prior to the start of collapse and R_{min} is the minimum radius of the bubble at the collapse. Therefore, it could be expected that the addition of Ar could drastically increase the temperature of cavitation bubbles, being beneficial to the sonochemical splitting of H_2O [77,78]. In addition, it could be found from Fig. S6 that, in the condition of Ar (80 %)-O_2(20 %), the generation of H_2O_2 in Pt_n(0.1 %)/SiO_2 sonocatalysis and pure ultrasound processes also increased to 261.5 μmol L^{-1} and 119.9 μmol L^{-1}, individually, but the increase was less than that of Pt_1(0.1 %)/SiO_2 sonocatalytic generation of H_2O_2. These experimental results further indicated that the thermal effect of Ar

in the ultrasonic process was much more beneficial to Pt_1 sonochemical catalysis of H_2O_2 generation. The stability of the enhancement effect of Ar(80 %)-O_2(20 %) mixed gas was also confirmed in Fig. 5d.

3.4. Enhancement mechanism of Pt_1 on the ultrasonic generation of H_2O_2

Many pieces of research have shown that the ultrasonic generation of H_2O_2 is a complex process [8,10,12,79]. Yean once presented 13 related chemical reactions [10], but they only involve two pathways: The first pathway is related to the ultrasonic splitting of water and the subsequent self-recombination of •OH (reaction (2)) [25]. The second pathway is dependent on the activation of O_2 and a series of radical reactions (reaction (3)–(4) and (7) [10]).

$$\bullet OOH + \bullet OOH = H_2O_2 + {}^1O_2 \tag{7}$$

Considering the ultrasonic is mainly associated with the initial reactions of the two pathways: water splitting and O_2 activation. Thus, the following investigations would mainly focus on the catalytic roles of Pt_1 towards the initial reactions (reaction (2)–(4)) in order to better understand the catalytic mechanism of Pt_1 in the ultrasonic generation of H_2O_2.

3.4.1. Promotion effect of Pt_1 on sonocatalytic splitting of water

Fig. 6a–c presented photographs of sonochemiluminescence in the Ar-saturated water for various sono-processes. It could be seen from these pictures that the intensity of sonochemiluminescence in the presence of Pt_1(0.1 %)/SiO_2 was much stronger than that in the presence of Pt_n(0.1 %)/SiO_2 and no catalyst (i.e. pure ultrasonic) process. It was well known that the intensity of sonochemiluminescence was directly proportional to the concentration of oxidative radicals. The difference between these sonochemiluminescences showed that Pt_1(0.1 %)/SiO_2 possessed a pronounced catalytic effect on the ultrasonic generation of the oxidative radicals, moreover, its catalytic effect was much more apparent than that of Pt_n(0.1 %)/SiO_2. According to the reaction (1)–(4), the oxidative radical from the ultrasonic splitting of water might be •OH, not others, in the Ar atmosphere due to no O_2. This possibility was confirmed by ESR spectra using DMPO as their spin trapping reagents in Ar atmosphere. When the no radical quenchers were added, nine ESR peaks with the intensity ratio of 1:2:1:2:1:2:1:2:1 were detected as indicated in Fig. 6d. They did not correspond to ESR peaks of any typical single radicals, rather than the complex ESR spectra reported by Wang et al. [20]. Moreover, when CCl_4 as •H quencher was added, four ESR peaks with the intensity ratio of 1:2:2:1 were detected (Fig. 6e). The features of ESR spectra were consistent with that of typical DMPO-•OH. When methanol as •OH quencher was added, nine ESR peaks with an

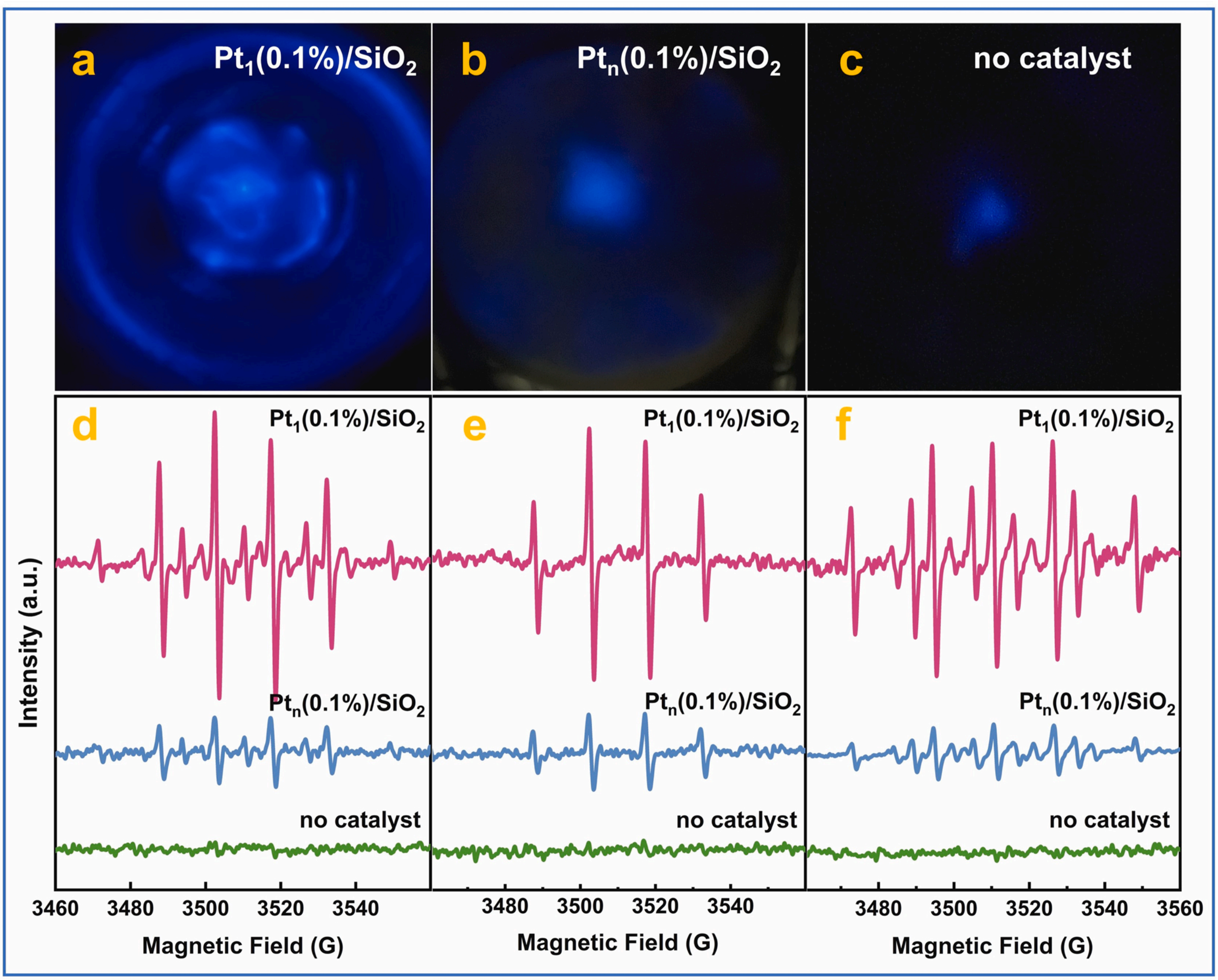

Fig. 6. Identification of radical generation in various sonocatalytic processes of H_2O in the Ar atmosphere (a, b, c: chemiluminescence of oxidation radicals, d: ESR of •OH and •H, ESR of •OH, e: ESR of •H).

intensity ratio of about 1:1:2:1:2:1:2:1:1 were detected (Fig. 6f). The features of ESR spectra were consistent with that of DMPO-•H [42,43]. These observations indicated that there were only •OH and •H, no other radical in the anaerobic Ar environment. In addition, the order of these ESR intensities for various catalytic processes was identical to that of the above sonochemiluminescence, i.e., Pt_1(0.1 %)/SiO_2 > Pt_n(0.1 %)/SiO_2 > > no catalyst (pure ultrasound). These facts confirmed that Pt_1 possessed a strong catalytic role in the ultrasonic splitting of water to •OH and •H in anaerobic environment.

DFT calculations were performed to theoretically investigate the interaction between Pt (Pt_1 or Pt_n) and H_2O. Fig. 7a and b presented the charge density differences of adsorbed H_2O on Pt_1/SiO_2(111) and Pt_8/SiO_2(111) from the DFT calculation. In the calculation, SiO_2(111) was used as the model adsorption crystal plane of SiO_2 and Pt_8 with 8 Pt atoms was as a model Pt_n for the convenience of the calculation. It could be seen from Fig. 7a and b that there were both charge transfers between the O atom of H_2O and Pt_1 or Pt_8, but the positive charge density of Pt_1 was apparently higher than that of Pt_8. The adsorption energy of Pt_1 and Pt_8 for H_2O was - 0.21 eV and - 0.58 eV, respectively. In other words, the adsorption energy of the unit Pt atom of Pt_1 and Pt_8 for H_2O was - 0.21 eV mole^{-1} and - 0.0725 eV mole^{-1}, separately. From this perspective, the adsorption energy of the unit Pt atom of Pt_1 for H_2O is 2.9 times that of Pt_8, indicating that Pt_1 interacted with H_2O more strongly than Pt_8. Moreover, the DFT calculation still showed that the activation energy or the dissociation barrier of the adsorbed H_2O splitting for Pt_1 catalysis was 0.19 eV mole^{-1}, which was much less than 0.59 eV mole^{-1} for Pt_8 catalysis. The former was only 32.2 % of the latter. Such a great difference suggested that the adsorbed H_2O on Pt_1 would be more rapidly cracked than on Pt_8 in view of reaction kinetics. Thus, the great catalytic activity of Pt_1 for the ultrasonic splitting of water into •OH could be attributed to the higher adsorption energy and smaller activation energy. They could be also regarded as the important reasons why Pt_1 enhanced the ultrasonic generation of H_2O_2 because it was frequently reported that the recombination of •OH was an important origin of H_2O_2 [25].

3.4.2. *Promotion effect of Pt_1 on the activation of O_2*

According to reaction (3) and (4), the combination of O_2 and •H from H_2O splitting could also generate H_2O_2. In other words, the activation of

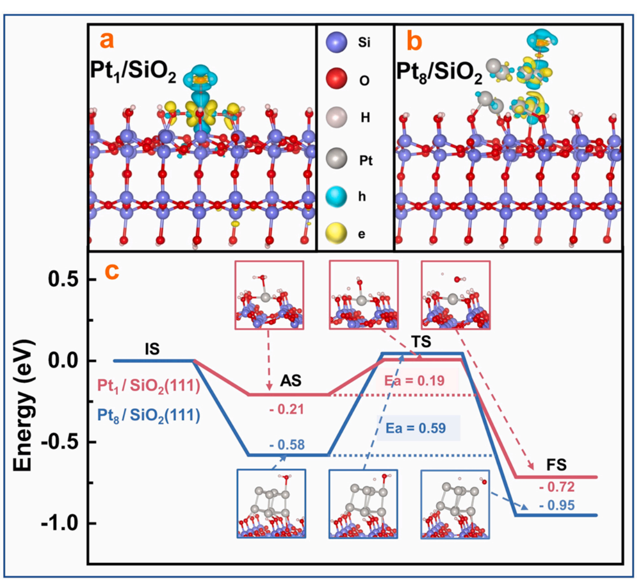

Fig. 7. Proposed reaction mechanism for H_2O dissolved on Pt_1/SiO_2 (a) and Pt_8/SiO_2 (b), charge density differences, and activation energy of adsorbed H_2O on Pt_1/SiO_2(111) and Pt_8/SiO_2(111) (c) (IS, AS, TS and FS stand for the initial state, adsorption state, transition state, and final state, separately).

Pt towards O_2 might be beneficial to the ultrasonic generation of H_2O_2. In order to quantitatively estimate the contribution of Pt to H_2O_2 generation by the pathway of O_2 activation, $O_2^{18,18}$ was used as the dissolved gas because the O element of H_2O was generally O^{16}. The isotopic determination showed that H_2O_2 contained about 32.1 % O^{18} in presence of Pt_1(0.1 %)/SiO_2 while only about 14.2 % O^{18} in the presence of Pt_n(0.1 %)/SiO_2. In other words, H_2O_2 originating from O_2 in presence of Pt_1(0.1 %)/SiO_2 was significantly higher than that in the presence of Pt_n(0.1 %)/SiO_2. These results clearly indicated that the activation of Pt_1 to O_2 was more beneficial to the ultrasonic generation of H_2O_2 than that of Pt_n.

Some researchers showed that the generation of H_2O_2 by the electrochemical reduction of O_2 was intensively dependent on the adsorption of O_2 on metal surfaces [80,81]. Generally, there are two kinds of adsorption models of O_2 on a metal surface, two side-on adsorption (Griffiths-type and Yeager-type) and one end-on adsorption (Pauling-type) [82–84]. On the surface of usual and nano metals, the adsorption of O_2 is mainly the two side-on type, which easily elongated and completely cleaved the O═O double bond, while the adsorption of O_2 molecule on atomically isolated sites was usually the end-on type, which could minimize the O-O bond breaking, thus facilitating the formation of •OOH intermediates by single-electron reduction [77,85–87] though H_2O_2 sono-generated from O_2 was by •H reduction, not single-electron reduction, as displayed in reaction (3) and (4), the interaction mechanism of O_2 and the surface of the metal catalysts should be similar. Therefore, it could be inferred that the atomically isolated Pt sites were beneficial to the one end-on adsorption of O_2 and the formation of •OOH as intermediates of H_2O_2, as shown in Fig. 8. The inference was confirmed by ESR determination in O_2-saturated water. As shown in Fig. 9a, in the presence of 60 % methanol, four ESR peaks (2 dual and 2 triple peaks) were observed. It was consistent with that of DMPO-•OOH adducts reported by Song [43,88]. It could be seen from the figure that the ESR peak of •OOH in the presence of Pt_1(0.1 %)/SiO_2 was much stronger than that in the presence of Pt_n(0.1 %)/SiO_2. The great difference could be as the supportive information as the end-on O_2 adsorption on Pt_1 and was also a key reason why Pt_1(0.1 %)/SiO_2 possessed the more effective than Pt_n(0.1 %)/SiO_2 in the sono-catalytic generation of H_2O_2 from O_2 because •OOH was the reaction product of the end-on adsorbed O_2 and •H (reaction (3)) and a crucial intermediate of the sono-catalytic generation of H_2O_2 from O_2, e.g., by the second pathway [38,39]. Fig. 9b presented the ESR characteristic peaks consistent with that of $^1O_2$. And the peak of $^1O_2$ from Pt_1(0.1 %)/SiO_2 catalytic process was much stronger than that from Pt_n(0.1 %)/SiO_2 catalytic process. Referring to Hayati's report [89], one of the sources of these $^1O_2$ species was the recombination reaction of •OOH, as indicated in reaction (7). Thus, the difference of $^1O_2$ the peak from Pt_1(0.1 %)/SiO_2 and Pt_n(0.1 %)/SiO_2 catalytic process was considerably dependent on the amount of •OOH. This further confirmed the above inference about the catalytic mechanism of Pt_1.

In addition, it was noticed that in the presence of Pt_1, the ultrasonic generation of H_2O_2 in the Ar(80 %)-O_2(20 %) atmosphere was 4.4 times in Ar (i.e. without O_2), as shown in Fig. 5c. This increasing value was much greater than the difference between the contents of H_2O_2 from H_2O and from O_2 (about 2.1 folds). Their inconsistency indicated the activation of Pt_1 for O_2 still had another pathway to increase H_2O_2 generation, in addition to reaction (3) and (4). Considering that many pieces of research showed that 80 % of •OH radicals from the ultrasonic splitting of water were scavenged by •H to recombine H_2O, and did not generate H_2O_2 [23,90]. Those facts showed that the increase of the combination of •H and the adsorbed O_2 on Pt_1 could not only promote H_2O_2 generation directly by the second pathway, as indicated in reaction (3) and (4), but also indirectly increased the generation of H_2O_2 from the first pathway by the capturing of these O_2 to •H to decrease recombination of •OH and •H to form H_2O. In other words, the first and second pathways possessed a synergistic enhancement effect.

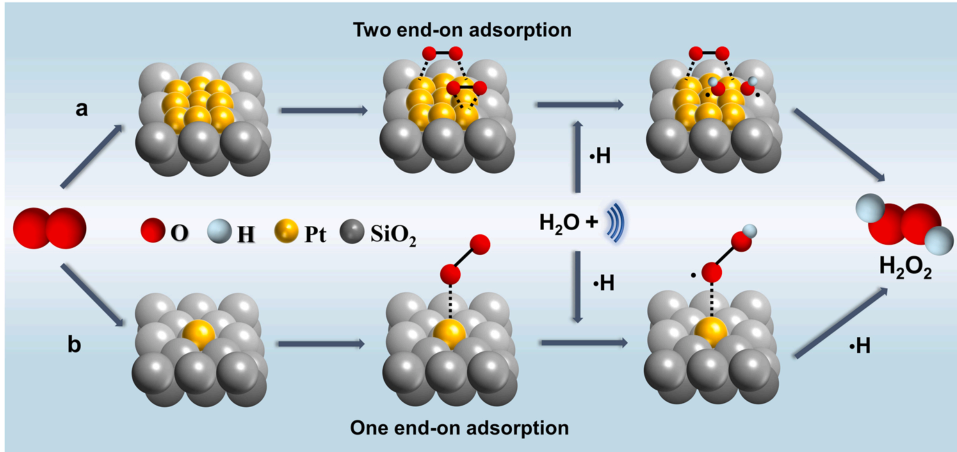

Fig. 8. Pathways of the ultrasonic formation of H_2O_2 from the adsorbed O_2 on the surface of Pt_1/SiO_2 and Pt_n/SiO_2.

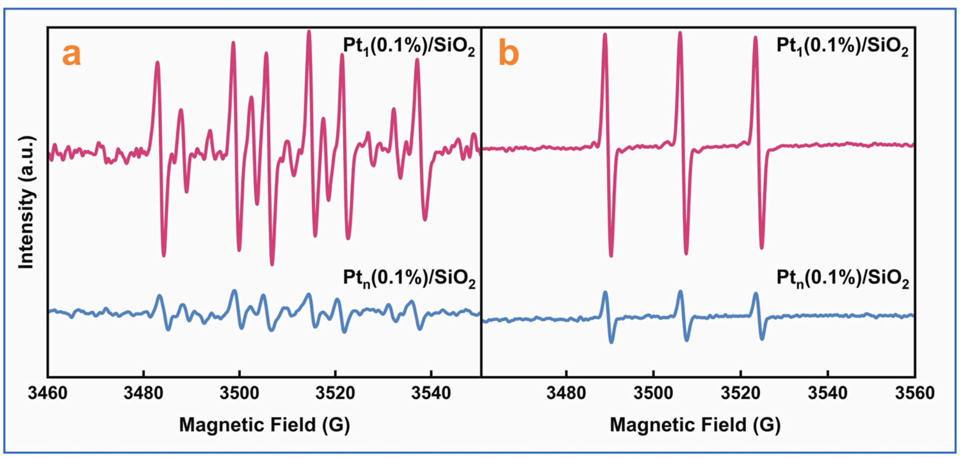

Fig. 9. ESR of •OOH(a) and $^1O_2$(b) from various sonocatalytic processes of Ar(80 %)-O_2(20 %)-saturated H_2O.

4. Conclusion

Pt_1 was first used to catalyze the sono-generation of H_2O_2. It was found that Pt_1(0.1 %)/SiO_2 could significantly boost the ultrasonic generation of H_2O_2, compared with both Pt_n(0.1 %)/SiO_2 and pure ultrasound. In the Ar(80 %)-O_2(20 %) atmosphere, the concentration of its H_2O_2 reached as high as 3027.1 μmol L^{-1} for 1 h, in which about 67.9 % originated from H_2O and about 32.1 % from O_2. The yield of H_2O_2 was 11.6 folds and 25.2 folds as those from Pt_n(0.1 %)/SiO_2 sonocatalysis and pure ultrasound process (Fig. S6). The great yield of H_2O_2 was attributed to the efficient two-way catalytic effect of Pt_1, namely the catalytic splitting of H_2O and the catalytic activation of O_2. For the splitting of H_2O process, Pt_1 had higher adsorption energy of H_2O and lower activation energy to split the adsorbed H_2O into •OH and •H. The activation of O_2 process was mainly dependent on Pt_1 selective activation to O_2 due to its special one end-on adsorption model for O_2. Moreover, it was still found that the two-way catalytic effect of Pt_1 could synergistically enhance the ultrasonic generation of H_2O_2. The findings of the strong catalytic effect and two-way catalytic mechanism of Pt_1 not only provided an effective way for the production of H_2O_2 but also extended the application of Pt_1 and deepened the understanding of ultrasonic catalytic processes and the size effect of Pt catalyst. Although the energy consumption of H_2O_2 generation in this work was lower than that of reported research in Table S2, this evaluation was based on lab-scale experiments and the focuses of these researches were different, thus, many investigations need to be performed before the H_2O generation process by Pt_1 sonic catalysis.

CRediT authorship contribution statement

Wen Yan: Methodology, Software, Validation, Investigation, Writing. **Jingxiang Sun:** Investigation, Data curation. **Tao Hu:** Conceptualization, Writing – review & editing. **Shuanghong Tian:** Conceptualization, Writing – review & editing. **Jinxi Feng:** Supervision, Conceptualization, Writing – review & editing, Funding acquisition. **Ya Xiong:** Project administration, Supervision, Conceptualization, Writing – review & editing, Funding acquisition.

Declaration of Competing Interest

The authors declare that they have no known competing financial interests or personal relationships that could have appeared to influence the work reported in this paper.

Acknowledgment

This research was supported by Natural Science Foundation of Guangdong Province (2021A1515012036), China Postdoctoral Science Foundation (2021M703675), the Fundamental Research Funds for the Central Universities, Sun Yat-Sen University (22qntd0901), National Natural Science Foundation of China (21976215), Guangzhou Municipal Science and Technology Project (202002030417) and Science and

Technology Projects of Guangdong Province (2019B1515120022).

Appendix A. Supporting information

Supplementary data associated with this article can be found in the online version at doi:10.1016/j.apcatb.2022.122143.

References

[1] R.S. Disselkamp, Energy storage using aqueous hydrogen peroxide, Energy Fuels 22 (2008) 2771–2774.
[2] S. Kato, J.U. Jung, T. Suenobu, S. Fukuzumi, Production of hydrogen peroxide as a sustainable solar fuel from water and dioxygen, Energy Environ. Sci. 6 (2013) 3756–3764.
[3] Y. Yamada, Y. Fukunishi, S. Yamazaki, S. Fukuzumi, Hydrogen peroxide as sustainable fuel: electrocatalysts for production with a solar cell and decomposition with a fuel cell, Chem. Commun. 46 (2010) 7334–7336.
[4] K. Jiang, J.J. Zhao, H.T. Wang, Catalyst design for electrochemical oxygen reduction toward hydrogen peroxide, Adv. Funct. Mater. 30 (2020) 2003321.
[5] J.M. Campos-Martin, G. Blanco-Brieva, J.L.G. Fierro, Hydrogen peroxide synthesis: An outlook beyond the anthraquinone process, Angew. Chem. Int. Ed. 45 (2006) 6962–6984.
[6] W. Zhou, L. Xie, J.H. Gao, R. Nazari, H.Q. Zhao, X.X. Meng, F. Sun, G.B. Zhao, J. Ma, Selective H_2O_2 electrosynthesis by O-doped and transition-metal-O-doped carbon cathodes via O_2 electroreduction: a critical review, Chem. Eng. J. 410 (2021), 128368.
[7] W.T. Richards, A.L. Loomis, The chemical effects of high frequency sound waves I. A preliminary survey, J. Am. Chem. Soc. 49 (1927) 3086–3100.
[8] Y. Nagata, K. Hirai, H. Bandow, Y. Maeda, Decomposition of hydroxybenzoic and humic acids in water by ultrasonic irradiation, Environ. Sci. Technol. 30 (1996) 1133–1138.
[9] Y. Jiang, C. Petrier, T.D. Waite, Sonolysis of 4-chlorophenol in aqueous solution: effects of substrate concentration, aqueous temperature and ultrasonic frequency, Ultrason. Sonochem. 13 (2006) 415–422.
[10] Y.L. Pang, A.Z. Abdullah, S. Bhatia, Review on sonochemical methods in the presence of catalysts and chemical additives for treatment of organic pollutants in wastewater, Desalination 277 (2011) 1–14.
[11] A.Z. Abdullah, P.Y. Ling, Heat treatment effects on the characteristics and sonocatalytic performance of TiO_2 in the degradation of organic dyes in aqueous solution, J. Hazard. Mater. 173 (2010) 159–167.
[12] I. Hua, M.R. Hoffmann, Optimization of ultrasonic irradiation as an advanced oxidation technology, Environ. Sci. Technol. 31 (1997) 2237–2243.
[13] S. Merouani, O. Hamdaoui, F. Saoudi, M. Chiha, Influence of experimental parameters on sonochemistry dosimetries: KI oxidation, fricke reaction and H_2O_2 production, J. Hazard. Mater. 178 (2010) 1007–1014.
[14] S. Ziembowicz, M. Kida, P. Koszelnik, The impact of selected parameters on the formation of hydrogen peroxide by sonochemical process, Sep. Purif. Technol. 204 (2018) 149–153.
[15] M. Sato, H. Itoh, T. Fujii, Frequency dependence of H_2O_2 generation from distilled water, Ultrasonics 38 (2000) 312–315.
[16] E. Dalodière, M. Virot, P. Moisy, S.I. Nikitenko, Effect of ultrasonic frequency on H_2O_2 sonochemical formation rate in aqueous nitric acid solutions in the presence of oxygen, Ultrason. Sonochem. 29 (2016) 198–204.
[17] C. Minero, P. Pellizzari, V. Maurino, E. Pelizzetti, D. Vione, Enhancement of dye sonochemical degradation by some inorganic anions present in natural waters, Appl. Catal. B-Environ. 77 (2008) 308–316.
[18] H.B. Zhang, C.S. Wei, Y.Y. Huang, J. Wang, Preparation of cube micrometer potassium niobate ($KNbO_3$) by hydrothermal method and sonocatalytic degradation of organic dye, Ultrason. Sonochem. 30 (2016) 61–69.
[19] J. Wang, Z.J. Pan, Z.H. Zhang, X.D. Zhang, F.Y. Wen, T. Ma, Y.F. Jiang, L. Wang, L. Xu, P.L. Kang, Sonocatalytic degradation of methyl parathion in the presence of nanometer and ordinary anatase titanium dioxide catalysts and comparison of their sonocatalytic abilities, Ultrason. Sonochem. 13 (2006) 493–500.
[20] Y.F. Wang, D. Zhao, W.H. Ma, C.C. Chen, J.C. Zhao, Enhanced sonocatalytic degradation of azo dyes by Au/TiO_2, Environ. Sci. Technol. 42 (2008) 6173–6178.
[21] A. Keck, E. Gilbert, R. Köster, Influence of particles on sonochemical reactions in aqueous solutions, Ultrasonic 40 (2002) 661–665.
[22] K.P. Jyothi, S. Joseph, S. Yesodharan, E.P. Yesodharan, Periodic change in the concentration of H_2O_2 formed during the semiconductor mediated sonocatalytic treatment of waste water; Investigations on pH effect and other operational variables, Res. J. Rec. Sci. 2 (2012) 1–14.
[23] C.H. Fischer, E.J. Hart, A. Henglein, Ultrasonic irradiation of water in the presence of oxygen $^{18,18}O_2$: isotope exchange and isotopic distribution of hydrogen peroxide, J. Phys. Chem. 90 (1986) 1954–1956.
[24] T. Chave, N.M. Navarro, P. Pochon, N. Perkas, A. Gedanken, S.I. Nikitenko, Sonocatalytic degradation of oxalic acid in the presence of oxygen and Pt/TiO_2, Catal. Today 241 (2015) 55–62.
[25] C. Minero, M. Lucchiari, D. Vione, V. Maurino, Fe(III)-enhanced sonochemical degradation of methylene blue in aqueous solution, Environ. Sci. Technol. 39 (2005) 8936–8942.
[26] P.Y. Fe, Ng, A. Brynjolfsson, J.W. Halliday, R.D. Jarrett, High-intensity radiolysis of aqueous ferrous sulfate-cupric sulfate-sulfuric acid solutions, J. Phys. Chem. 74 (1970) 1221–1227.
[27] B.T. Qiao, A.Q. Wang, X.F. Yang, L.F. Allard, Z. Jiang, Y.T. Cui, J.Y. Liu, J. Li, T. Zhang, Single-atom catalysis of CO oxidation using Pt_1/FeO_x, Nat. Chem. 3 (2011) 634–641.
[28] Y.T. Shi, C.Y. Zhao, H.S. Wei, J.H. Guo, S.X. Liang, A.Q. Wang, T. Zhang, J.Y. Liu, T.L. Ma, Single-atom catalysis in mesoporous photovoltaics: the principle of utility maximization, Adv. Mater. 26 (2014) 8147–8153.
[29] H. Wang, J.X. Liu, L.F. Allard, S. Lee, J.L. Liu, H. Li, J.Q. Wang, J. Wang, S. Oh, W. Li, M. Flytzani-Stephanopoulos, M.Q. Shen, B.R. Goldsmith, M. Yang, Surpassing the single-atom catalytic activity limit through paired Pt-O-Pt ensemble built from isolated Pt_1 atoms, Nat. Commun. 10 (2019) 3808.
[30] Y.L. Wang, S. Gurses, N. Felyey, A. Boubnov, S.S. Mao, C.X. Kronawitter, In situ deposition of Pd during oxygen reduction yields highly selective and active electrocatalysts for direct H_2O_2 production, ACS Catal. 9 (2019) 8453–8463.
[31] C.H. Choi, H.C. Kwon, S. Yook, H. Shin, H. Kim, M. Choi, Hydrogen peroxide synthesis via enhanced two-electron oxygen reduction pathway on carbon-coated Pt surface, J. Phys. Chem. C 118 (2014) 30063–30070.
[32] X.Z. Song, N. Li, H. Zhang, H. Wang, L.Y. Wang, Z.Y. Bian, Promotion of hydrogen peroxide production on graphene-supported atomically dispersed platinum: Effects of size on oxygen reduction reaction pathway, J. Power Sources 435 (2019), 226771.
[33] G.M. Liu, Y. Huang, H.Q. Lv, H. Wang, Y.B. Zeng, M.Z. Yuan, Q.G. Meng, C. Y. Wang, Confining single-atom Pd on g-C_3N_4 with carbon vacancies towards enhanced photocatalytic NO conversion, Appl. Catal. B-Environ. 284 (2021), 119683.
[34] S.F. Ji, Y.J. Chen, G.F. Zhao, Y. Wang, W.M. Sun, Z.D. Zhang, Y. Lu, D.S. Wang, Atomic-level insights into the steric hindrance effect of single-atom Pd catalyst to boost the synthesis of dimethyl carbonate, Appl. Catal. B-Environ. 304 (2022), 120922.
[35] Z.W. Huang, T. Ban, Y. Zhang, L.P. Wang, S.F. Guo, C.R. Chang, G.H. Jing, Boosting the thermal stability and catalytic performance by confining Ag single atom sites over antimony-doped tin oxide via atom trapping, Appl. Catal. B-Environ. 283 (2021), 119625.
[36] H.R. Song, R. Du, Y.W. Wang, D.Y. Zu, R. Zhou, Y. Cai, F.X. Wang, Z. Li, Y.M. Shen, C.P. Li, Anchoring single atom cobalt on two-dimensional MXene for activation of peroxymonosulfate, Appl. Catal. B-Environ. 286 (2021), 119898.
[37] Z.Y. Jiang, M.Z. Jing, X.B. Feng, J.C. Xiong, C. He, M. Douthwaite, L.R. Zheng, W. Y. Song, J. Liu, Z.G. Qu, Stabilizing platinum atoms on CeO_2 oxygen vacancies by metal-support interaction induced interface distortion: Mechanism and application, Appl. Catal. B-Environ. 278 (2020), 119304.
[38] E. Yeager, Recent advances in the science of electrocatalysis, J. Electrochem. Soc. 128 (1981) 160–171.
[39] E. Yeager, Dioxygen electrocatalysis: mechanisms in relation to catalyst structure, J. Mol. Catal. 38 (1986) 5–25.
[40] W.Y. Zhu, S.W. Chen, Recent progress of single-atom catalysts in the electrocatalytic reduction of oxygen to hydrogen peroxide, Electroanalysis 32 (2020) 2591–2602.
[41] X. Guo, S. Lin, J. Gu, S. Zhang, S. Huang, Simultaneously achieving high activity and selectivity toward two-electron O_2 electroreduction: The power of single-atom catalysts, ACS Catal. 9 (2019) 11042–11054.
[42] Y.F. Wang, D. Zhao, H.W. Ji, G.L. Liu, C.C. Chen, W.H. Ma, H.Y. Zhu, J.C. Zhao, Sonochemical hydrogen production efficiently catalyzed by Au/TiO_2, J. Phys. Chem. C 114 (2010) 17728–17733.
[43] H.Y. Song, L.S. Wei, C.X. Chen, C.C. Wen, F.Q. Han, Photocatalytic production of H_2O_2 and its in situ utilization over atomic-scale Au modified MoS_2 nanosheets, J. Catal. 376 (2019) 198–208.
[44] J.X. Feng, J.X. Sun, X.S. Liu, J.Z. Zhu, Y. Xiong, S.H. Tian, Enhancement and mechanism of nano-$BaTiO_3$ piezocatalytic degradation of tricyclazole by co-loading Pt and RuO_2, Environ. Sci. Nano 6 (2019) 2241–2252.
[45] C. Kormann, D.W. Bahnemann, M.R. Hoffmann, Photocatalytic production of hydrogen peroxides and organic peroxides in aqueous suspensions of titanium dioxide, zinc oxide, and desert sand, Environ. Sci. Technol. 22 (1988) 798–806.
[46] C. Kong, Y. Yoon, Y.D. Choi, S.J. Lee, J. Oh, J. Han, N. Her, Sonocatalytic degradation of naphthalene and phenol in the presence of inert glass beads and single-walled carbon nanotubes, J. Nanoelectron. Optoelectron 7 (2012) 522–529.
[47] J. Savarino, M.H. Thiemens, Analytical procedure to determine both $\delta^{18}O$ and $\delta^{17}O$ of H_2O_2 in natural water and first measurements, Atmos. Environ. 33 (1999) 3683–3690.
[48] G. Kresse, J. Hafner, Ab initio molecular-dynamics simulation of the liquid-metal-amorphous-semiconductor transition in germanium, Phys. Rev. B 49 (1994) 14251–14269.
[49] G. Kresse, J. Furthmuller, Efficient iterative schemes for ab initio total-energy calculations using a plane-wave basis set, Phys. Rev. B 54 (1996) 11169–11186.
[50] G. Kresse, D. Joubert, From ultrasoft pseudopotentials to the projector augmented-wave method, Phys. Rev. B 59 (1999) 1758–1775.
[51] S.P. Ding, Y.L. Guo, M.J. Hulsey, B. Zhang, H. Asakura, L.M. Liu, Y. Han, M. Gao, J. Y. Hasegawa, B.T. Qiao, T. Zhang, N. Yan, Electrostatic stabilization of single-atom catalysts by ionic liquids, Chem. -Us 5 (2019) 3207–3219.
[52] W. Zhang, H.Z. Wang, J.W. Jiang, Z.J. Sui, Y.A. Zhu, D. Chen, X.G. Zhou, Size dependence of Pt catalysts for propane dehydrogenation: From atomically dispersed to nanoparticles, ACS Catal. 10 (2020) 12932–12942.
[53] Z.X. Zeng, Y. Su, X. Quan, W.Y. Choi, G.H. Zhang, N. Liu, B. Kim, S. Chen, H.T. Yu, S.S. Zhang, Single-atom platinum confined by the interlayer nanospace of carbon nitride for efficient photocatalytic hydrogen evolution, Nano Energy 69 (2020), 104409.

[54] D.F. Hou, Z.F. Jiao, Z.P. Liang, Y.W. Wang, X.N. Guo, X.Y. Guo, Selectivity control of Pt/SiC catalysts for photothermocatalytic hydrogenation of 3-nitrostyrene, Appl. Surf. Sci. 526 (2020), 146616.
[55] P.D. Nellist, S.J. Pennycook, Direct imaging of the atomic configuration of ultradispersed catalysts, Science 274 (1996) 413–415.
[56] P.D. Nellist, M.F. Chisholm, N. Dellby, O. Krivanek, M. Murfitt, Z. Szilagyi, A. R. Lupini, A. Borisevich, W. Sides Jr, S. Pennycook, Direct sub-angstrom imaging of a crystal lattice, Science 305 (2004), 1741 – 1741.
[57] A.A. Herzing, C.J. Kiely, A.F. Carley, P. Landon, G.J. Hutchings, Identification of active gold nanoclusters on iron oxide supports for CO oxidation, Science 321 (2008) 1331–1335.
[58] M. Kottwitz, Y.Y. Li, R.M. Palomino, Z.Y. Liu, G.J. Wang, Q. Wu, J.H. Huang, J. Timoshenko, S.D. Senanayake, M. Balasubramanian, D.Y. Lu, R.G. Nuzzo, A. I. Frenkel, Local structure and electronic state of atomically dispersed Pt supported on nanosized CeO_2, ACS Catal. 9 (2019) 8738–8748.
[59] S.P. Ding, H.A. Chen, O. Mekasuwandumrong, M.J. Hulsey, X.P. Fu, Q. He, J. Panpranot, C.M. Yang, N. Yan, High-temperature flame spray pyrolysis induced stabilization of Pt single-atom catalysts, Appl. Catal. B-Environ. 281 (2021), 119471.
[60] P. Bera, K.R. Priolkar, A. Gayen, P.R. Sarode, M.S. Hegde, S. Emura, R. Kumashiro, V. Jayaram, G.N. Subbanna, Ionic dispersion of Pt over CeO_2 by the combustion method: Structural investigation by XRD, TEM, XPS, and EXAFS, Chem. Mater. 15 (2003) 2049–2060.
[61] X.H. He, Q. He, Y.C. Deng, M. Peng, H.Y. Chen, Y. Zhang, S.Y. Yao, M.T. Zhang, D. Q. Xiao, D. Ma, B.H. Ge, H.B. Ji, A versatile route to fabricate single atom catalysts with high chemoselectivity and regioselectivity in hydrogenation, Nat. Commun. 10 (2019) 3663.
[62] C.L. Wang, X.K. Gu, H. Yan, Y. Lin, J.J. Li, D.D. Liu, W.X. Li, J.L. Lu, Water-mediated mars-van krevelen mechanism for CO oxidation on ceria-supported single-atom Pt_1 catalyst, ACS Catal. 7 (2017) 887–891.
[63] H. Shin, W.-G. Jung, D.-H. Kim, J.-S. Jang, Y.H. Kim, W.-T. Koo, J. Bae, C. Park, S.-H. Cho, B.J. Kim, Single-atom Pt stabilized on one-dimensional nanostructure support via carbon nitride/SnO_2 heterojunction trapping, ACS Nano 14 (2020) 11394–11405.
[64] T.Z. Xu, H. Zheng, P.Y. Zhang, Isolated Pt single atomic sites anchored on nanoporous TiO_2 film for highly efficient photocatalytic degradation of low concentration toluene, J. Hazard. Mater. 388 (2020), 121746.
[65] V. Srinivasa Rao, M.S. Reddy, K.T.S.S. Raju, B.H. Babu, Investigation of intermolecular interactions in binary liquid mixtures of [Bmim][NTf_2] and propylene carbonate at different temperatures using ultrasonic, optical and FT-IR studies, Karbala Int. J. Mod. Sci. 3 (2017) 279–286.
[66] C. Zhu, S. Fu, Q. Shi, D. Du, Y. Lin, Single-atom electrocatalysts, Angew. Chem. Int. Ed. 56 (2017) 13944–13960.
[67] G. Kyriakou, M.B. Boucher, A.D. Jewell, E.A. Lewis, T.J. Lawton, A.E. Baber, H. L. Tierney, M. Flytzani-Stephanopoulos, E.C.H. Sykes, Isolated metal atom geometries as a strategy for selective heterogeneous hydrogenations, Science 335 (2012) 1209–1212.
[68] N. Her, J.S. Park, Y. Yoon, Sonochemical enhancement of hydrogen peroxide production by inert glass beads and TiO_2-coated glass beads in water, Chem. Eng. J. 166 (2011) 184–190.
[69] K. Yasui, T. Tuziuti, Y. Iida, H. Mitome, Theoretical study of the ambient-pressure dependence of sonochemical reactions, J. Phys. Chem. 119 (2003) 346–356.
[70] P. Kanthale, M. Ashokkumar, F. Grieser, Sonoluminescence, sonochemistry (H_2O_2 yield) and bubble dynamics: frequency and power effects, Ultrason. Sonochem. 15 (2008) 143–150.
[71] Y. Asakura, K. Yasuda, Frequency and power dependence of the sonochemical reaction, Ultrason. Sonochem. 81 (2021), 105858.
[72] M. Lim, Y. Son, J. Khim, The effects of hydrogen peroxide on the sonochemical degradation of phenol and bisphenol A, Ultrason. Sonochem. 21 (2014) 1976–1981.
[73] M. Sivakumar, P.A. Tatake, A.B. Pandit, Kinetics of p-nitrophenol degradation: effect of reaction conditions and cavitational parameters for a multiple frequency system, Chem. Eng. J. 85 (2002) 327–338.
[74] A.M. Basedow, K.H. Ebert, Ultrasonic degradation of polymers in solution, Phys. Chem. 22 (1977) 83–148.
[75] P.N.V. Laxmi, P. Saritha, N. Rambabu, V. Himabindu, Y. Anjaneyulu, Sonochemical degradation of 2chloro-5methyl phenol assisted by TiO_2 and H_2O_2, J. Hazard. Mater. 174 (2010) 151–155.
[76] E.J. Hart, A. Henglein, Free radical and free atom reactions in the sonolysis of aqueous iodide and formate solutions, J. Phys. Chem. 89 (1985) 4342–4347.
[77] K. Okitsu, T. Suzuki, N. Takenaka, H. Bandow, R. Nishimura, Y. Maeda, Acoustic multibubble cavitation in water: A new aspect of the effect of a rare gas atmosphere on bubble temperature and its relevance to sonochemistry, J. Phys. Chem. B 110 (2006) 20081–20084.
[78] R. Pflieger, T. Chave, G. Vite, L. Jouve, S.I. Nikitenko, Effect of operational conditions on sonoluminescence and kinetics of H_2O_2 formation during the sonolysis of water in the presence of Ar/O_2 gas mixture, Ultrason. Sonochem. 26 (2015) 169–175.
[79] S. Ziembowicz, M. Kida, P. Koszelnik, Sonochemical formation of hydrogen peroxide, Proceedings 2 (2018) 188.
[80] C.H. Chu, D.H. Huang, Q.H. Zhu, E. Stavitski, J.A. Spies, Z.H. Pan, J. Mao, H.L. L. Xin, C.A. Schmuttenmaer, S. Hu, J.H. Kim, Electronic tuning of metal nanoparticles for highly efficient photocatalytic hydrogen peroxide production, ACS Catal. 9 (2019) 626–631.
[81] F.C. Zhang, W.W. Xie, N. Zhang, S. Li, X. Wang, Understanding catalytic activity trends of atomic pairs in single-atom catalysts towards oxygen reduction reactions, Appl. Surf. Sci. 598 (2022), 153873.
[82] J.S. Griffith, On the magnetic properties of some hæmoglobin complexes, Proc. R. Soc. Lond. Ser. A 235 (1956) 23–36.
[83] E. Yeager, M. Razaq, D. Gervasio, A. Razak, A.D. Tryk, The electrolyte factor in O2 reduction electrocatalysis. Proceedings of the workshop on structural effects in electrocatalysis and oxygen electrochemistry, The Electrochemical Society Inc., Pennington, NJ, 1992, pp 440–473.
[84] L. Pauling, Nature of the iron-oxygen bond in oxyhmoglobin, Nature 203 (1964) 182–183.
[85] M.M. Montemore, M.A. van Spronsen, R.J. Madix, C.M. Friend, O_2 activation by metal surfaces: Implications for bonding and reactivity on heterogeneous catalysts, Chem. Rev. 118 (2018) 2816–2862.
[86] M.L. Pegis, C.F. Wise, D.J. Martin, J.M. Mayer, Oxygen reduction by homogeneous molecular catalysts and electrocatalysts, Chem. Rev. 118 (2018) 2340–2391.
[87] A. Wang, J. Li, T. Zhang, Heterogeneous single-atom catalysis, Nat. Rev. Chem. 2 (2018) 65–81.
[88] M. Pinteala, S. Schlick, Direct ESR detection and spin trapping of radicals generated by reaction of oxygen radicals with sulfonated poly(ether ether ketone) (SPEEK) membranes, Polym. Degrad. Stabil. 94 (2009) 1779–1787.
[89] F. Hayati, S. Moradi, S.F. Saei, Z. Madani, S. Giannakis, A.A. Isari, B. Kakavandi, A novel, Z-scheme ZnO@AC@FeO photocatalyst, suitable for the intensification of photo-mediated peroxymonosulfate activation: Performance, reactivity and bisphenol A degradation pathways, J. Environ. Manag. 321 (2022), 115851.
[90] K. Makino, M.M. Mossoba, P. Riesz, Chemical effects of ultrasound on aqueous solutions. Formation of hydroxyl radicals and hydrogen atoms, J. Phys. Chem. 87 (1983) 1369–1377.